Modelling the effect of hydraulic stimulation strategies on fault reactivation and induced seismicity

Brecht Wassing[1], Quan Gan[2], Thibault Candela[1], Daniel Loeve[1] and Peter A. Fokker[1]

[1] TNO, Utrecht, the Netherlands

[2] University of Aberdeen, Address, Scotland, UK

brecht.wassing@tno.nl

Keywords: Enhanced geothermal systems, hydraulic stimulation, fault reactivation, induced seismicity.

ABSTRACT

Hydraulic stimulation is frequently used to enhance the permeability of natural fracture networks in deep low-permeability rocks. The downside of hydraulic stimulation of pre-existing fractures is that it may trigger felt induced seismicity through reactivation. For a successful development of enhanced geothermal systems, it is crucial to stimulate rocks to enhance flow rate, whilst keeping magnitudes of induced earthquakes at acceptable levels by means of so-called 'soft' hydraulic stimulation.

Here we use a 3D coupled Thermal-Hydraulic-Mechanical model in Tough2-FLAC3D to simulate the effect of different stimulation strategies on the characteristics of fault reactivation and induced seismicity. Using the Tough2-FLAC3D simulator, we take into account the full coupling between the hydraulic and mechanical processes affecting flow through the reservoir and the mechanical response of the fault system. We model fluid injection into a single well, at close distance to a single fault, bounded by a fault damage zone and embedded in a fractured rock matrix. For different injection scenarios, we analyze the impact on fault stress changes, fault stressing rates and associated seismicity. We discuss the effect of the different stimulation strategies on the evolution of induced seismicity both during and after hydraulic stimulation. We also discuss the effect of fault transmissibility on induced seismicity and effectiveness of the stimulation strategies.

1. INTRODUCTION

Hydraulic stimulation is frequently used to enhance the permeability of natural fracture networks in deep low-permeability rocks. The downside of hydraulic stimulation is that it may trigger or induce felt seismicity. For a successful development of enhanced geothermal systems, it is crucial to stimulate the rocks in order to enhance flow rates, whilst keeping magnitudes of induced earthquakes at acceptable levels. Recently in the literature, soft stimulation strategies have been proposed as an option to mitigate induced seismicity during hydraulic stimulation. The concept of soft hydraulic stimulation has been described by Zang et al (2013), Zimmermann et al (2015) and Huenges et al (2017), whereas Hofmann et al (2018, 2019) describe the application of a soft hydraulic stimulation scheme at the Pohang EGS site in Korea. Soft hydraulic stimulation may encompass a range of stimulation techniques, including techniques such as cyclic and multistage stimulation. Other measures such as the application of a gradual shut-in of the injection well to avoid a fast release of poroelastic stresses and associated seismicity after shut-in (as suggested by Segall et al (2015)), well bleed-off and flowback, or the application of a gradual increase of injection rates from the start of injection may also be regarded as techniques which are meant to mitigate seismicity associated to the hydraulic stimulation operations.

In the present paper, we use a 3D coupled hydro-mechanical model in Tough-Flac3D (Taron and Elsworth 2010, Gan and Elsworth 2014) in combination with the rate-and-state seismicity theory of Dieterich (1994) to investigate the effect of different hydraulic stimulation strategies on fault reactivation and associated seismicity. In a recent paper Chang and Yoon 2018 have shown that the presence of low-permeability faults at close distance to the well can affect pressure and poroelastic changes, and thereby influence fault reactivation and seismicity. In this study, we focus on the impact of fault transmissivity at the evolution of seismicity in space and time.

2. MODELLING APPROACH

Using the Tough2-FLAC3D simulator, we take into account the full coupling between the hydraulic and mechanical processes affecting flow through the reservoir and the mechanical response of the fault system. We model injection into a single well, at close distance to a steep fault of 70º dip, which is bounded by a fault damage zone and embedded in a fractured rock matrix. We test the impact of the permeability of the fault zone, i.e. we vary the permeability of the fault and analyze the impact on fault stresses, loading rates and related seismicity, both during the injection period and after shut-in of the injection well. At present we are not aiming at modelling a specific field case, though chosen conditions can be considered as being more or less representative of some of the geological conditions encountered at a number of EGS sites, where geothermal systems often target the high-permeability damage zones of fault structures in the crystalline basement or low-permeability clastic reservoirs (e.g. as

in some of the EGS sites in the Lower Rhine Graben, where injection wells are generally located in close vicinity of a large fault structure (Vidal and Genter 2018) or the Pohang EGS site where one of the injection wells was probably located within or very close to the damage zone of a large fault structure (Hofmann et al 2018, 2019, Kim et al 2017, Grigoli et al 2017).

We model a 70º dipping fault of 1 km length and 3 km width, located at a depth between 3700 m and 4700m below surface level. The model grid is aligned with the strike of the fault. The model geometry is presented in Fig.1. Dimensions of the model are 3 km x 3 km x 2 km. Vertical model boundaries are fixed horizontally and the lower horizontal boundary is fixed in a vertical direction, whereas a vertical stress is imposed on the upper model boundary, which represents the weight of the overburden. The modelled fault (core) is surrounded by a highly permeable damage zone embedded in a low-permeability rock matrix. The width of the damage zone is 50 m. The fluid is injected close to the damage zone, and a direct hydraulic connection (e.g. due to the presence of a hydraulic fracture or pre-existing fracture) exists between the damage zone and the injection well. Water is injected directly into the damage zone within the hanging wall block of the fault, at a distance of approximately 50 m from the fault. To analyze the effect of fault transmissibility on fault stress changes, three scenarios for the transmissibility of the fault core have been analyzed: a fault with low transmissibility ('sealing fault'), a fault with intermediate transmissibility ('partially sealing fault') and a fault with high transmissibility ('open fault'). In case of the open fault, no distinction is made between the permeabilities of the fault and the damage zone. Fault, damage zone and rock matrix are characterized by uniform permeability and homogeneous elastic properties. Elastic properties for the fault, damage zone and matrix are a Young's modulus of 33 GPa and a Poisson's ratio of 0.25, and a Biot coefficient of 0.8.

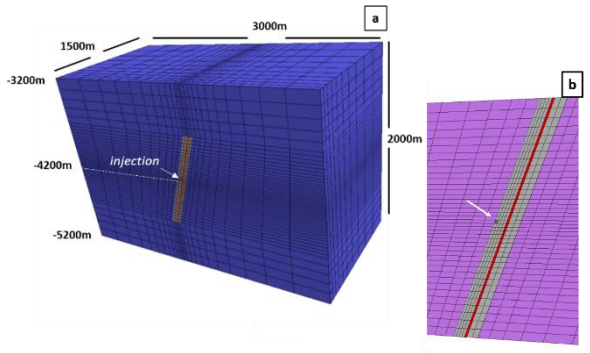

Figure 1: a) Geometry of the fault (red), damage zone (grey) and matrix rocks (blue); b) detail of the fault zone and location of injection. Half of the model shown (model has been cut by a vertical plane oriented perpendicular to the y-axis, through the injection point).

Porosity and permeability for the rock matrix is 0.01 and 1e-16 m^2 respectively. Porosity and permeability of the damage zone is 0.05 and 3e-15 m^2 respectively. Porosity and permeability of the fault zone is varied: In case of an *open fault*, the fault zone is considered to represent one single fracture zone, and porosity and permeability of fault core and damage zone are assumed to be equal. In addition, we modelled a *sealing fault* (low porosity and permeability of 0.001 and 2e-19 m^2) and a *partially sealing fault* (porosity and permeability of 0.001 and 8e-16m^2).

The initial stress regime is a strike slip tectonic regime, with $SH_{max} > S_v > sh_{min}$ and maximum horizontal stress SH_{max} oriented at an oblique angle (approximately 70°) to the strike of the fault (i.e. representative of right-lateral strike slip conditions). Water pressures are assumed to be hydrostatic; total maximum horizontal stress gradient is assumed to be 31 MPa/km, total minimum horizontal stress gradient is 19 MPa/km and total vertical stress gradient is 26 MPa/km.

The impact of varying hydraulic stimulation scenarios on fault stability and associated seismicity has been analyzed. The injection scenarios are based on some of the main features of the soft hydraulic stimulation for the Pohang site, as described by Hofmann et al. (2018, 2019). Three scenarios have been analyzed; in all three cases total volumes injected before shut-in are 2000 m^3 and maximum injection rates are 10 l/s. In scenario 1) injection rates are rapidly increased up to a constant rate of 10 l/s, followed by a sharp shut-in; Scenario 2 follows the main pattern of scenario 1, with constant injection rates of 10 l/s, but with a gradual shut-in of the injection well ('tapered shut-in'). Injection scenario 3) is a cyclic injection, with 4 cycles of injection, and rates varying between 5 and 10 l/s.

At all fault locations, the spatio-temporal evolution of pore pressures and normal- and shear stresses on the fault are monitored. Pore pressures, and normal and shear stresses on the fault plane are used to calculate Coulomb stress changes. Coulomb stresses changes ($\Delta\tau_{cs}$) are caused by both the increase of pore pressures due to diffusion into the fault (which is here referred to as the direct pore pressure effect) and poroelastic stress changes caused by the deformation of the rocks, and can be written as:

$$\Delta\tau_{cs} = \Delta(\tau_s - \mu\sigma'_n) \qquad [1]$$

Or in terms of total stresses:

$$\Delta\tau_{cs} = (\Delta\tau_s - \mu\Delta\sigma_n + \mu\Delta P) \qquad [2]$$

Where Δ denotes a change, τ_s is shear stress, σ'_n is normal effective stress on the fault, σ_n is total normal stress on the fault, μ is friction coefficient of the fault and P is pore pressure in the fault. Positive Coulomb stress changes indicate a destabilizing stress path of the fault, whereas a fault segment with negative Coulomb stress changes is stabilizing. The first two components of equation [2] denote the contribution of poroelastic stress changes on the fault, the last component of

equation [2] gives the contribution of the direct pore pressure effect.

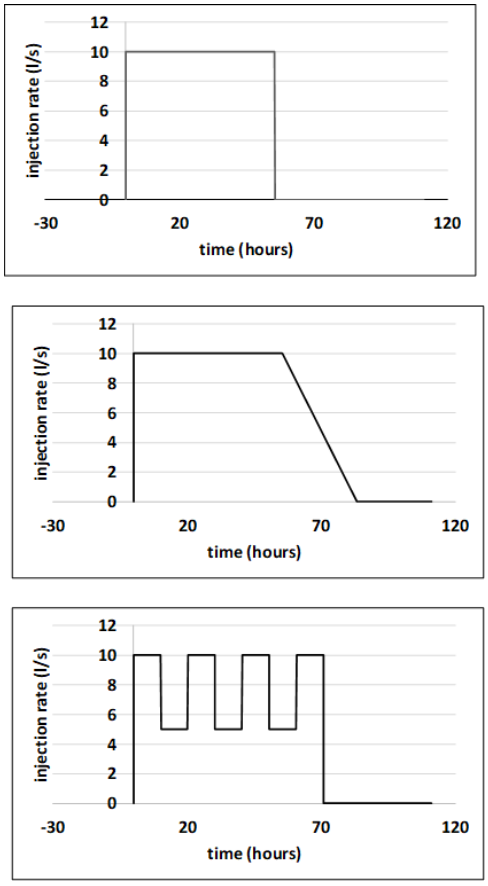

Figure 2: Prescribed injection scenarios applied in simulations, from top to bottom Sc1) constant injection with sudden shut-in, Sc2) constant injection with tapered shut-in, Sc3) cyclic injection.

From the evolution of Coulomb stress changes over time, Coulomb stressing rates can be derived. Coulomb stressing rates are then used to obtain relative seismicity rates, based on the theory of rate-and-state seismicity (Dieterich 1994, Segall et al 2015):

$$\frac{dR}{dt} = \frac{R}{t_a}\left(\frac{\dot{\tau}_{cs}}{\dot{\tau}_0} - R\right) \qquad [3]$$

In which R is relative seismicity rate (seismicity rate divided by background seismicity rate) and τ_0 is tectonic stressing rate. The t_a is a decay parameter, which defines how long it takes for seismicity to decay to its background value, following a large stress perturbation. The magnitude of t_a depends on background stressing rate, fault parameter A which quantifies the direct effect of rate and state friction behavior of the fault and normal effective stress:

$$t_a = \frac{A\dot{\tau}_0}{\sigma_n'} \qquad [4]$$

In this study we assume A = 0.001, and τ_0 of 0.0002 MPa/yr, which results in $t_a \approx 100$ years. As shown by Ader et al (2014) and Segall et al (2015) the time decay factor t_a will affect the delay between stress perturbations and the seismic response of the fault. Ader et al (2014) have shown that for a very short t_a relative to the duration of the perturbation, the predicted seismicity rate will resemble the pattern of Coulomb stressing rates, whereas for very large t_a (relative to the perturbation), predicted seismicity rates will follow the trend of the Coulomb stress changes.

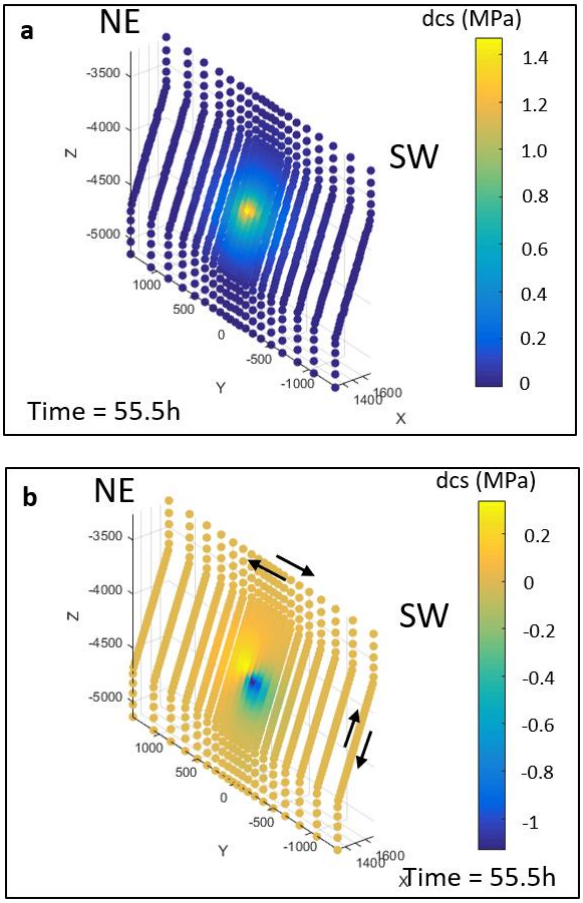

Figure 3: Sc1 - Coulomb stress changes at the end of the injection phase (55.5h), just before shut-in. a) for open fault and b) for sealing fault.

3. MODELLING RESULTS

The total period of injection analysed for all scenarios is 120 hours, which means we will not evaluate the long-term effects of pore pressure diffusion into the fault. Modelling results for the 3 scenarios are summarized in the sections below:

3.1 Scenario 1: constant injection with immediate shut-in of the injection well.

Injection period. Fig.3 presents the distribution of Coulomb stress changes at the end of the injection period, just before shut-in of the injection well, i.e. for an open fault (a) and a sealing fault (b). Distributions of Coulomb stresses on the fault differ, with a radially distributed pattern on the open fault, and an asymmetrical distribution for the sealing fault and partially sealing fault (not shown here).

Individual components of changes in pore pressure, total normal stress and shear stress versus time, at the fault location closest to the injection well, are presented in Fig.4. Looking at the contribution of the pore pressures, normal stresses and shear stresses to the Coulomb stress changes, we can observe from Fig.4 that:

Regarding the effect of pore pressure changes: In case of the open fault, the major contribution to Coulomb stress changes is from the pore pressure increase itself, as pore pressures can rapidly diffuse into the fault (Fig.4a). For the sealing fault (Fig.4b), for the short-term injection-period modelled, contributions from pore pressures are negligible. For the partially sealing fault (Fig.4c) significant pore pressure effects are observed during the injection period, albeit smaller than in case of the open fault.

Regarding the effect of shear stress changes: In case of the sealing fault, the contribution of shear stresses to Coulomb stressing is large (Fig.4b). For the partially sealing fault (Fig.4c) the change in shear stress is significant, but smaller than in case of the sealing fault. For the open fault (Fig.4a), changes in shear stresses are small. The evolution of shear stresses can explain the asymmetry observed in the pattern of Coulomb stress changes on the fault in Fig.3b, for both the sealing and partially sealing fault. As poroelastic volumetric expansion of the rocks occurs solely in the hanging wall block of the fault, this will cause additional shear stresses on the upper segment of the fault above and to the NE of the injection well, adding to the shear stresses already present from the tectonic loading. Increments in shear stresses on the lower and SW fault segment however counteracted the in-situ tectonic shear stresses, which led to a stabilizing effect on this part of the fault. In case of the open fault, and to a lesser extent also for the partially sealing fault, rock volumes on both sides of the fault expand, resulting in smaller differential movements along the fault and a less significant contribution of the shear stresses.

Regarding the effect of normal stress changes: In contrast to shear stresses, changes in total normal stresses at the end of the injection period are largest for the open fault (Fig.4a), as rock volumes expand on both sides of the fault, whereas volumetric expansion for the sealing fault (fig.4b), and (to a lesser extent) the partially sealing fault (Fig.4c) is limited to, and 'smeared out' over the matrix rocks and damage zone in the hanging wall block.

Regarding Coulomb stress changes: Total Coulomb stress changes are largest for the open fault (Fig.4a), mainly due to the large increase in pore pressures. In summary, Coulomb stressing for the open fault is dominated by direct pressure effects, whereas for the sealing fault Coulomb stressing is dominated by poroelastic effects (shear), with large normal stresses at the injection level and below leading to negative Coulomb stress changes and fault stabilization at the injection level shown in Fig.4b and below. In case of the partially sealing fault both poroelastic and direct pressure effects play a role, and contribute equally to Coulomb stressing (Fig.4c).

After shut-in. For the open fault, after shut-in, changes in Coulomb stresses in the area around the injection well are negative (see Fig.4a). Shut-in of the well thus leads to a rapid stabilization of the fault in the near-well area. In case of the sealing fault, the effect of pore pressures decreasing is minimal; here the response after shut-in is dominated by the immediate release of poroelastic stresses.

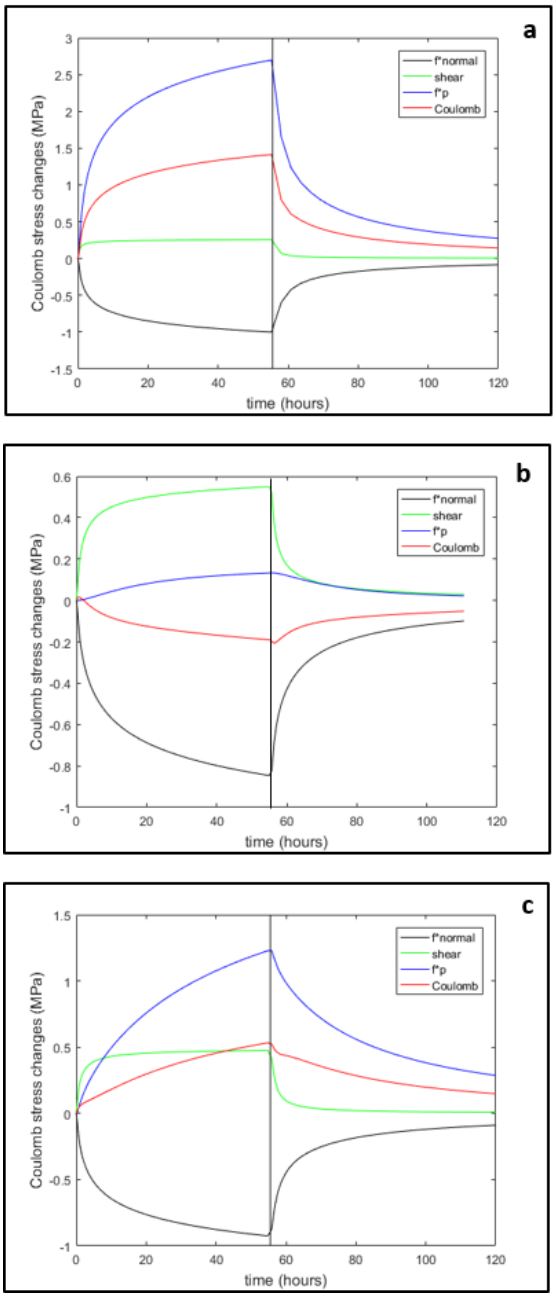

Figure 4: Contribution of pressure (blue), normal (black)- and shear stress (green) to Coulomb stress changes (red) for a) open fault, b) sealing fault and c) partially sealing fault. Coulomb stress evolution at the fault location nearest to the injection well is shown. Black vertical line is moment of shut-in.

The release results in an increase of Coulomb stresses due to unclamping of the fault, but effects are too small to induce positive Coulomb stresses at the injection level (Fig.4b).

Locally, the response for the partially sealing fault after shut-in is different: Fig.5 shows the effect of immediate shut-in of the injection well on post shut-in fault stresses and seismicity for the partially sealing fault, at a location just below the injection level. Here, although shear stresses and pore pressures do diminish, the clamping forces of the normal stresses reduce significantly. The latter being the largest and immediate effect, a rapid but temporary increase of Coulomb stresses in the near-well fault segment is observed. This effect has also been described in a recent publication of Segall and Lu (2015).

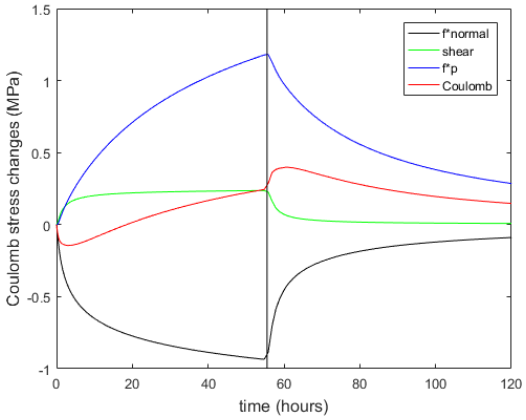

Figure 5: Contribution of pore pressure, normal stress and shear stress to Coulomb stress changes for the partially sealing fault, at the fault location, just below the injection level. Black vertical line is moment of shut-in.

Coulomb stressing- and seismicity rates. The evolution of Coulomb stress changes can be used to derive Coulomb stressing rates and associated seismicity rates, as e.g. shown in Fig.6 for the open fault(top) and partially sealing fault (bottom). Values are plotted for three different locations, i.e. at the location of largest Coulomb stress changes (blue), at the location of largest seismicity rates (green) and at the location nearest to the injection point (injection level, red, which is the same location as used for plotting Coulomb stress evolution in Fig.4). For the open fault (top), maximum Coulomb stress changes, maximum stressing rates and maximum seismicity rates all occur at the fault location nearest to the injection point, so the three curves overlap. As can be observed from Fig.6 bottom, in case of the partially fault maximum Coulomb stresses and maximum seismicity rates do not occur at the same fault location, neither at the location nearest to the injection well. For the partially sealing fault Fig.6c (bottom) clearly shows a sharp peak in seismicity rate after shut-in of the injection well, related to the sudden increase in Coulomb stresses after shut-in shown in Fig.5. This is the location where largest seismicity rates are observed for the partially sealing fault (green). For other locations, seismicity rates reached their peak right after the onset of the stimulation see (e.g. red and blue curve).

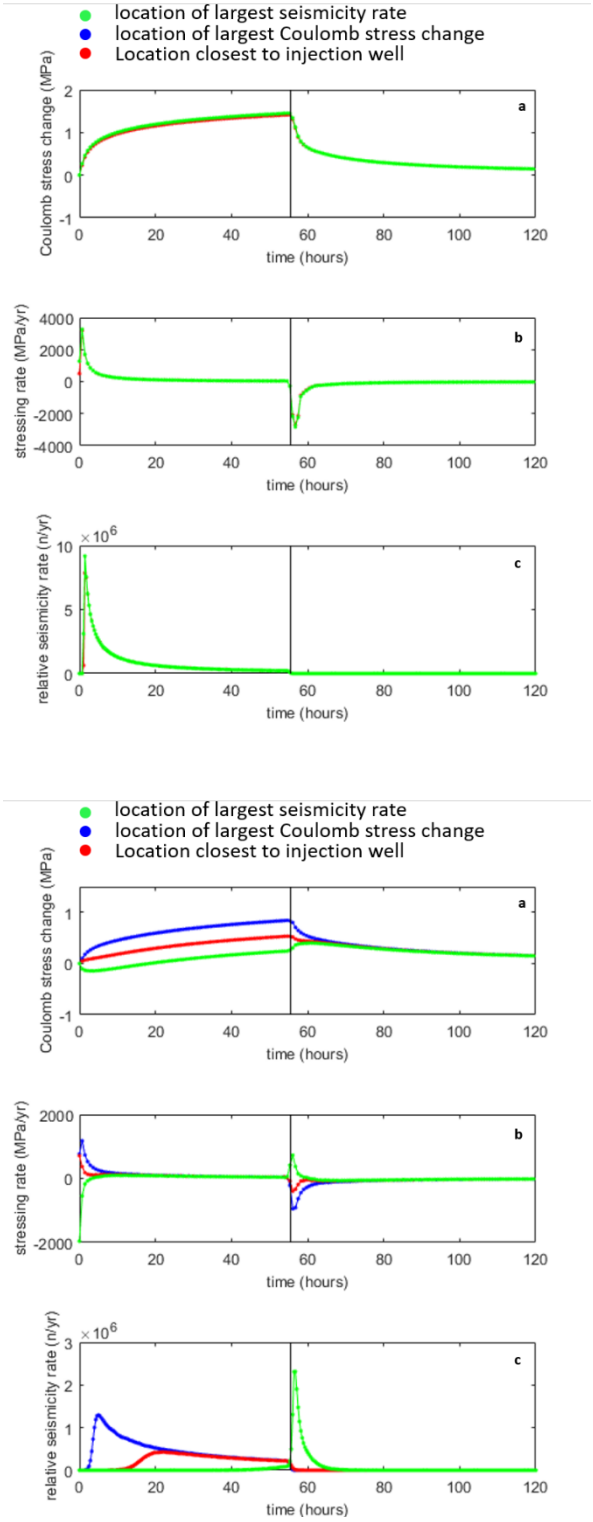

Figure 6: Top: open fault and bottom: partially sealing fault. Shown a) Coulomb stress changes, b) Coulomb stressing rates and c) seismicity rates during the first 120 hours of injection. Color-coded curves represent the response at 3 different locations at the fault (see legend above graph).

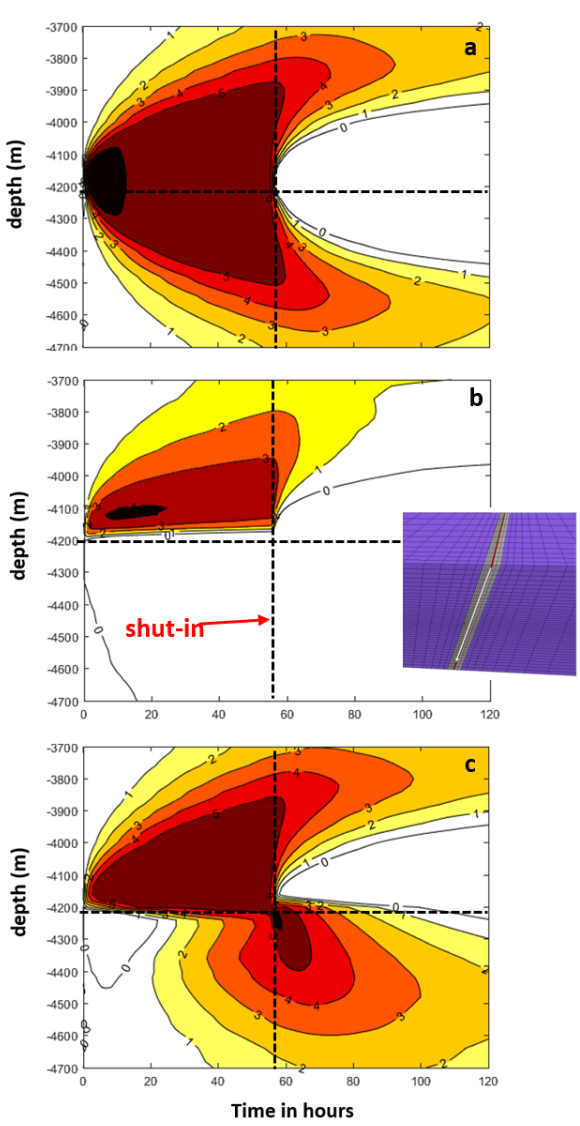

Figure 7: Seismicity rate versus time for a) open fault, b) sealing fault and c) partially sealing fault. Seismicity is plotted along a line oriented in the dip direction of the fault plane, close to the injection point in the centre of the model. White arrow in inlay shows location of line for plotting.

The spatial and temporal evolution of seismicity rates for the three fault transmissivities are shown in Fig.7. This figure presents the seismicity rates which occur along a line oriented along the dip direction of the fault, close to the injection point at the centre of the model (see inlay Fig.7). In case of the open fault, largest stressing rates occur just after the start of injection as the fault almost directly feels the rise in pore pressures. Seismicity shows a similar pattern, with highest event rates occurring within the first few hours after the injection starts (here shown for a t_a of ≈100 years), concentrated in the near-well fault area (Fig.7a). For the sealing fault seismicity peaks somewhat later during the injection phase and event rates are lower, as Coulomb stresses build up slower (Fig.3b) and stressing rates are lower than for the open fault (Fig. 3-b). Seismicity is only observed on the upper fault segment above and to the NE of the injection well (Fig.7-b). For both the open and sealing fault, immediate shut-in of the injection well results in an aseismic zone in the near-well fault area, which extends further outwards in time. For the partially sealing faults, seismicity during injection shows an intermediate pattern as compared to the open and sealing fault (Fig 7-c): Seismicity is observed soon after the start of injection, with event rates lying between the rates observed for the open and sealing fault. Seismicity during injection is predominantly located on the upper NE fault segment, but the lower fault segment is reactivated during the later stages of injection. The behaviour at shut-in is strikingly different from the other two scenarios, with highest event rates occurring just after shut-in and located below the injection interval. This can be directly related to the immediate, but temporary increase in Coulomb stresses and high Coulomb stressing rates just after shut-in of the injection well (see also Fig 6c, green curve).

3.2 Scenario 2: constant injection with tapered shut-in of the injection well.

To analyze the effect of a gradual shut-in on seismicity after shut-in, the effect of tapering of the shut-in phase has been analyzed for the partially sealing fault. Obviously, during the injection phase scenario 2 shows a similar pattern for Coulomb stressing, stressing rates and induced seismicity rates as scenario 1 (Fig.8). After shut-in, a gradual tapered shut-in of the injection helps in reducing the post-shut-in peak of seismicity (Fig.8c, green curve). Segall and Lu 2015 have shown the effectiveness of the slow shut-in to be dependent on the duration of shut-in and the rate-and-state properties of the fault (t_a).

3.3 Scenario 3: cyclic injection

Pore pressure changes and maximum Coulomb stress changes for the open fault are lower for cyclic injection, as pore pressures are allowed to dissipate over a longer period. Maximum seismicity rates reached during the first injection cycle equal maximum seismicity rates for constant injection. For cyclic injection the duration of the first seismicity peak is shorter. Four peaks in Coulomb stressing rates and associated peaks of event rates are observed during the injection period, which are directly related to the onset of the individual cycles, when rates are increased from 5 to 10 l/s. Similar to the constant injection rates, the highest seismicity peak is observed soon after the start of the first cycle; the heights of the peaks for the following cycles decline rapidly. Intervals of negligible to low seismicity rates are related to intervals of low (5 l/s) injection rates (Kaiser effect, Fig. 9 and Fig.10). Similar to constant injection, Coulomb stresses and seismicity rates rapidly decline after shut-in of the injection. As compared to constant injection, the effect of cyclicity on reduction of seismic event rates appears to be limited.

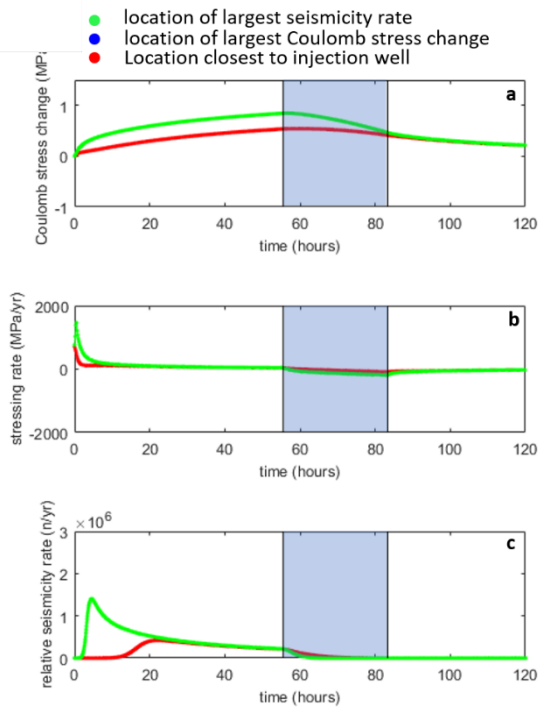

Figure 8: Seismicity rates for the partially sealing fault after shut-in. Color-coded curves are representative for 3 locations at the fault (see legend above graph). Shaded area indicates tapering period.

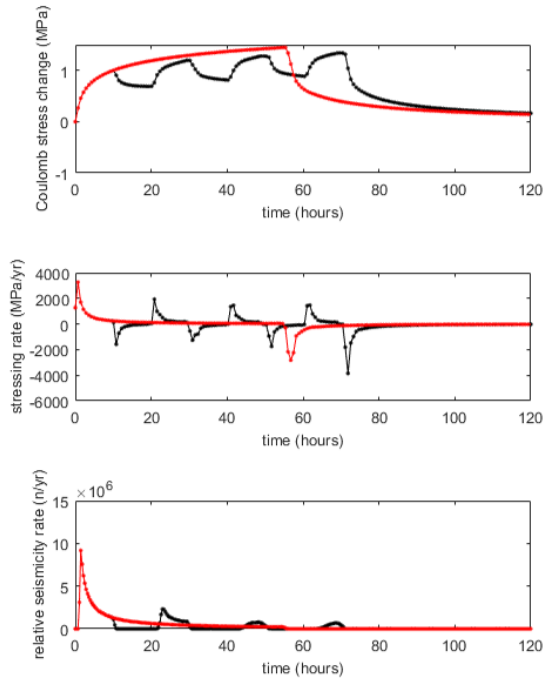

Figure 9: Open fault: Comparison of constant (red) versus cyclic (black) injection. a) Coulomb stress change, b) Coulomb stressing rates, c) seismicity rates.

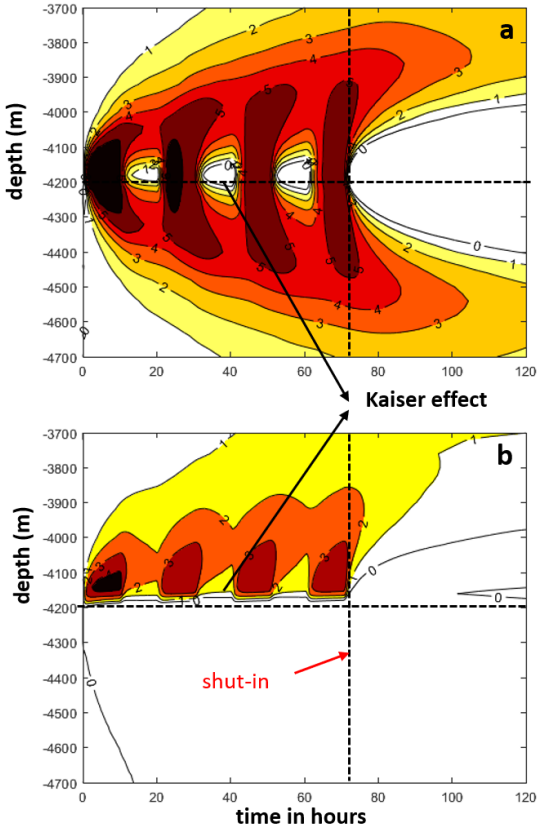

Figure 10: Seismicity rates versus time for cyclic injection, a) open fault and b) sealing fault.

4. DISCUSSION AND CONCLUSIONS

The hydro-mechanically coupled model in Tough-FLAC3D enables the evaluation of the effect of hydraulic stimulation strategies on fault Coulomb stress changes, stressing rates and associated seismicity rates. The relative contribution of direct pressure and poroelastic effects on fault stressing, which affects the 3D spatial and temporal distribution and evolution of Coulomb stressing (rates) and seismicity, can be analysed. In a recent paper Chang and Yoon 2018 have shown that the presence of low-permeability faults at close distance to the well can affect pressure and poroelastic changes, and thereby influence fault reactivation and seismicity. Here we studied the role of the fault transmissivity in determining the spatio-temporal pattern of seismicity.

Regarding the temporal evolution of seismicity, modelling results show that the direct pore pressure effects dominate the seismic response of the fault in case of an open fault, causing highest stressing rates and seismicity rates just after the start of injection. For the sealing fault, poroelastic effects are dominant, with high shear stressing rates and seismicity rates after the onset of injection. The partially sealing fault shows an intermediate response, with poroelastic and direct pore pressure effects almost equally balanced. For the partially sealing fault, the fast reduction of (clamping) normal stresses on the fault after shut-in of the well overrules the positive effects of pressure reduction and

decrease of shear stresses. This results in a post shut-in rise of seismic event rates. As shown, post shut-in seismicity rates can be reduced by a tapering of the shut-in of the injection well.

We also see that the permeability of the fault drives the spatial pattern of seismicity. For this specific fault geometry, located in a right-lateral strike-slip tectonic setting and an injection well in the hanging wall block of the fault, we find that during injection a low fault permeability promotes the occurrence of seismicity on the fault segment located above and to the NE of the injection interval. In case of a high fault permeability, seismicity shows a more symmetrical concentric spatial distribution around the near-well area. As mentioned before, when the poroelastic effect of clamping and unclamping dominates the response of the fault, as in case of the partially sealing fault, peaks in seismicity rates after shut-in can be expected. For the particular setup studied here with its injection characteristics, fault geometry and tectonic setting, the sharp increase in post shut-in seismicity was observed mainly on the fault segment below and to the SW of the injection point.

A gradual shut-in of the injection well does indeed reduce the peaks of high post shut-in seismicity rates, and can in that sense be regarded as a successful mitigation measure. For the particular setup studied here, the effects of cyclic injection on reduction of seismicity rates are limited. However, in this study we only focus on seismicity rates, whereas the total number of seismic events or event magnitudes might provide a better measure of seismic hazard. As discussed by Hofmann et al (2018, 2019), processes like stress relaxation caused by plasticity and creep, and mechanical fatigue which results in a lowering of fracture break-down pressures, may play an important role during cyclic stimulation. These mechanical processes cannot be captured in the current elastic model. Other potential soft stimulation techniques such as application of a gradual increase of injection rates at the start of the hydraulic stimulation and applying flowback to ensure zero net injected volumes have not yet been analysed. Such topics can be focus of future studies.

It is noted here that next to fault transmissibility, other subsurface properties such as damage zone and matrix flow properties, mechanical properties such as stiffness of the fault core, damage zone and matrix, as well as fault geometry, location and distance of the injection well to the fault and the tectonic setting, will have an effect on the relative contribution of poroelastic and direct pore pressure effects, and hence also on the spatial and temporal distribution of the seismicity. Moreover, the timing and shape of the seismicity peaks will be determined by the rate-and-state fault parameters (e.g. t_a). In practice many of these parameters will be uncertain, and difficult to determine prior to the hydraulic stimulation operations. However, the results of this study indicate that modelling combined with a close monitoring of the spatial and temporal distribution of seismicity may help to further constrain some of the unknown subsurface parameters, such as e.g. fault transmissivity.

REFERENCES

Ader, Th., Lapusta, N., Avouac, J.P. and Ampuero, J.P.: Response of rate-and-state seismogenic faults to harmonic shear-stress perturbations, *Geophys. J. Int.* (2014), 198, 385-413.

Chang, K.W., Yoon H.: 3-D Modeling of Induced Seismicity along Multiple Faults: Magnitude, Rate and Location in a Poroelasticity System, *J. Geophys. Res. Solid Earth* (2018), 123.

Dieterich, J.: A constitutive law for rate of earthquake production and its application to earthquake clustering. *J. of Geophys. Research* (1994), 99 B2, 2601-2618.

Gan, Q. and Elsworth, D. Thermal drawdown and late-stage seismic-slip fault reactivation in enhanced geothermal reservoirs. *J. Geophys. Res. Solid Earth* (2014), 119, 8936-8949.

Grigoli F., Cesca, S., Rinaldi, A.P., Manconi, A.,Lopez-Comino, J.A., Clinton, J.F., Westaway, R., Cauzzi, C., Dahm, T. and Wiemer, S.: The November 2017 Mw 5.5 Pohang earthquake: A possible case of induced seismicity in South Korea. *Science* 10.1126/science.aat2010 (2018).

Huenges, E., Zang, A., Kim, K.Y.: Soft stimulation and induced seismicity, Schatzalp workshop on Induced seismicity, Davos, Switzerland, 14-17, (2017).

Hofmann, H., Zimmermann, G., Zang, A., Min, K.B.: Cyclic Soft stimulation (CCS0: A new fluid injection protocol and traffic light system to mitigate seismic risks of hydraulic stimulation treatments, *Geotherm Energy* (2018), 6:27.

Hofmann, H., et al.: First field application of cyclic soft stimulation at the Pohang Enhanced Geothermal system site in Korea, *Geophys. Intern.* 217, pp 926-949 (2019).

Kim, K.H., Ree, J.H., Kim, J.H., Kim, S., Kang, S.Y., Seo, W.: Assessing whether the 2017 Mw 5.4 Pohang earthquake in South Korea was an induced event. et al 2018. *Science* 10.1126/science.aat6081 (2018).

Segall, P., Lu, S.: Injection-induced seismicity: Poroelastic and earthquake nucleation effects. *J. Geophys. Res. Solid Earth* (2015), 120, 5082-5103.

Taron, J. and Elsworth, D.: Coupled mechanical and chemical processes in engineered geothermal reservoirs with dynamic permeability, International journal of rock Mechanics and Mining Sciences (2010, 47, 1339-1348.

Vidal J. and Genter A.: Overview of naturally permeable fractured reservoirs in the central and southern Upper rhine Graben: Insights from geothermal wells, *Geothermics* (2018), 74, 57-73.

Zang, A., Yoon, J.S., Stephansson, O. and Heidbach, O.: fatigue hydraulic fracturing by cyclic reservoir treatment enhances permeability and reduces induced seismicity, *Geophys. J. Int.* (2013), 195(2), 1282-1287.

Zimmermann, G., Hofmann, H., Babdagli, T., Yoon, S.J., Zang, A., Deon, F., Urpi, L., Blocher, G., Hassanzadegan, A., and Huenges, E.: Multi-fracturing and cyclic hydraulic stimulation scenarios to develop enhanced geothermal systems – feasibility and mitigation strategies to reduce seismic risk, *Proceedings of the World Geothermal Congress 2015*, Melbourne, Australia, 19-25 April (2015), paper #31009.

Acknowledgements

The project leading to part of the results in this article received funding from the European Union's Horizon 2020 research and innovation programme under grant agreement No 691728.